Revista Internacional de Investigación e Innovación Tecnológica

Página principal: www.riiit.com.mx

Magnesium ferrite nanoparticles as cancer treatment adjuvants: synthesis, characterization, and heating capacity

Nanopartículas de ferrita de magnesio como coadyuvantes del tratamiento del cáncer: síntesis, caracterización y capacidad de calentamiento

García-Feria, C.[a], Reséndiz-Hernández, P.J.[a]*, Cortés-Hernández, D.A.[b], Ochoa-Palacios, R.M.[a]

[a] División de Estudios de Posgrado e Investigación, Tecnológico Nacional de México/ I. T. de Saltillo, Blvd. Venustiano Carranza 2400, Col. Tecnológico, Saltillo 25280, Coahuila, México.
[b] Cinvestav-Unidad Saltillo, Av. Industria Metalúrgica #1062, Parque Industrial Saltillo-Ramos Arizpe, Ramos Arizpe 25900, Coahuila, México.
gferiacarolina@gmail.com; perla.rh@saltillo.tecnm.mx*; dora.cortes@cinvestav.edu.mx; rocio.op@saltillo.tecnm.mx

Technological innovation: Synthesis of nanoparticles that can be used in cancer therapy by means of magnetic hyperthermia.

Industrial application area: Biomedical.

Received: november 02th, 2024
Accepted: may 06th, 2025

Resumen

Se utilizó un método de síntesis por vía húmeda, mediante microemulsión para obtener nanopartículas magnéticas con la fórmula general $MgxFe_{3-x}O_4$, donde x = 0.2, 0.4, 0.6, 0.8 y 1. Después de evaluar las propiedades magnéticas y la capacidad de calentamiento de los polvos sintetizados, se encontró que los resultados más adecuados corresponden a los valores de x = 0.8 y 1. El análisis de XRD reveló una estructura de espinela que corresponde a la fase pura de $MgFe_2O_4$; formada gracias a los cationes metálicos de magnesio (Mg^{2+}) reemplazando a los iones metálicos de hierro (Fe^{3+} - Fe^{2+}). Usando la técnica SEM-EDX, se encontraron agregados de nanopartículas que variaban entre de 5 a 20 µm (tratadas a 900°C). Los resultados del análisis por TGA-DSC indicaron pérdidas del 50% del material precursor y mostraron el inicio de la formación de la fase cristalina a los 500 °C. El análisis por TEM confirma la existencia de la fase de $MgFe_2O_4$, con morfología esférica y un tamaño promedio de partícula de 31 nm. El análisis VSM demostró un comportamiento superparamagnético; en donde el valor de magnetización de saturación máximo

encontrado en las nanopartículas ($MgFe_2O_4$) fue de 18.52 emu/g. La prueba de inducción magnética de estado sólido reveló que el uso de 6,0 mg de nanopartículas por tabla de solución permite elevar la temperatura del medio (H_2O) a 44.32 °C en menos de 10 minutos. Los niveles de citotoxicidad para células eritrocitarias en presencia de ferritas de magnesio fueron superiores al 50% hasta por 60 horas. Con base en los resultados, estas nanopartículas podrían ser efectivas en el tratamiento del cáncer mediante terapia de hipertermia magnética, ya que son capaces de alcanzar temperaturas que inducen inestabilidad térmica en proteínas y nutrientes en la zona afectada, lo que conduce a la muerte de las células neoplásicas. A diferencia de las células normales, las células cancerosas presentan mayor sensibilidad a las variaciones de temperatura.

Palabras clave: Ferritas, Hipertermia, Microemulsión, Nanopartículas, Superparamagnético.

Abstract

A microemulsion wet synthesis method was employed to obtain magnetic nanoparticles with the general formula $MgxFe_{3-x}O_4$, where x = 0.2, 0.4, 0.6, 0.8, and 1. After evaluating the magnetic properties and heating capacity of the synthesized powders, it was found that the most suitable results correspond to the values of x = 0.8 and 1. XRD analysis revealed a spinel structure corresponding to the pure phase of $MgFe_2O_4$, formed due to magnesium metal cations (Mg^{2+}) replacing iron metal ions (Fe^{3+} - Fe^{2+}). Using the SEM-EDX technique, aggregates of nanoparticles ranging from 5 to 20 µm were found (heat treatment at 900 °C). The results of the TGA-DSC analysis indicated a 50% loss of the precursor material and showed the onset of crystalline phase formation at 500 °C. TEM analysis confirms the presence of the $MgFe_2O_4$ phase, with a spherical morphology and an average particle size of 31 nm. VSM analysis demonstrated superparamagnetic behavior, where the maximum saturation magnetization value found in the nanoparticles ($MgFe_2O_4$) was 18.52 emu/g. The solid-state magnetic induction test revealed that using 6.0 mg of nanoparticles per ml of solution allows the temperature of the medium (H_2O) to rise to 44.32 °C in less than 10 minutes. Cytotoxicity levels for erythrocyte cells in the presence of magnesium ferrites were up to 60 hours higher than 50% and very close to the control used. Based on the results, these nanoparticles could be effective in cancer treatment through magnetic hyperthermia therapy, as they can reach temperatures that induce thermal instability in proteins and nutrients in the affected area, leading to the death of neoplastic cells. Unlike normal cells, cancer cells exhibit greater sensitivity to temperature variations.

Keywords: Ferrites, Hyperthermia, Microemulsion, Nanoparticles, Superparamagnetic.

1. Introduction

Soft nanoferrites are compounds characterized by the general formula $MO{\cdot}Fe_2O_3$ and a cubic crystal structure, where M denotes a divalent metal ion such as Mg^{2+}, Fe^{2+}, Mn^{2+}, Ni^{2+}, or Zn^{2+}. These materials exhibit an inverse spinel structure, a variation of the original spinel mineral ($MgO \cdot Al_2O_3$) [1]. Due to their unique magnetic properties, soft nanoferrites are widely utilized in applications including ferrofluids,

magnetic hyperthermia, biosensing technologies, and targeted drug delivery systems [1][2].

Magnesium ferrite is often synthesized in the field of nanoferrites using a combination of wet synthesis techniques, including microemulsion [3][4], coprecipitation [5], and sol-gel [3]. Microemulsions are liquid systems composed of water, oil, surfactants, and occasionally co-surfactants**,** and are commonly used in nanoparticle synthesis. This process offers several advantages, including precise control over particle size and distribution, ease of production, and thermodynamic stability. From a biological perspective, magnesium ions are the predominant divalent cations within the cytoplasm. They are the only ones present at concentrations exceeding the millimolar range in their |unbound, free form [2] [4].

The materials used for nanoparticles can combine both therapeutic and diagnostic properties within a single formulation, with one notable example being cancer therapy [5][6][7]. Cancer is a type of tissue growth that is caused by the proliferation of abnormal cells that are capable of infiltrating and destroying other tissues. The most common cause of cancer is aberrant activity or mutations in the biological genes that control cell division and growth [8][9][10][11]. Exposure of magnetic nanoparticles to an alternating current magnetic field causes them to reach a temperature of 41–46 °C, which kills tumor cells. This is known as magnetic hyperthermia. This therapy is an appealing alternative for destroying cancer cells due to its ability to generate localized heat in a specific area [12][7][13][14].

Magnesium-based nanoparticles have been investigated as potential agents in various biological systems. According to Rangnath *et al.*[15]. The use of nanoferrites as heating agents with applications in magnetic hyperthermia has been explored [13][14]. The outcomes of this study may make lasting contributions to the advancement of research in this field.

2. Materials and methods

2.1 Materials

The chemical reagents employed in this study included: magnesium nitrate hexahydrate $Mg(NO_3)_2$ $6H_2O$, iron (III) chloride hexahydrate $FeCl_3 \cdot H_2O$, n-hexane C_6H_{14} (99.7% - J.T. Baker), ammonium hydroxide NH_4OH, n-butanol CH_3 $(CH_2)_2$ CH_2OH (99%), Brij 35 (Polyoxyethylene (23) lauryl ether) $C_{12}H_{25}(OCH_2CH_2)_{23}OH$ (99%), and distilled water.

2.2 Synthesis of $MgFe_2O_4$ nanoparticles by microemulsion method

The synthesis of magnesium ferrites was initiated. 1. 5 grams of Brij 35 were dissolved in a mixture of hexane and butanol 2. The mixture was stirred for 30 minutes. 3. The aqueous solutions of iron chloride and magnesium nitrate ($Mg_xFe_{3-x}O_4$, where x = 0.2, 0.4, 0.6, 0.8, or 1) were prepared and incorporated into the initial mixture while stirring for 10 min. 4. Incorporation of the NH_4 dropwise for 30 minutes. 5. Mixing for further 15 minutes, trying to maintain a pH of 11. 6. Rinsing with distilled water followed by precursor preparation through decantation. 7. Aging for 24 h at 100 °C. 8. Grinding of the dried material is followed by heat treatment at 900 °C for 2 h (Figure 1).

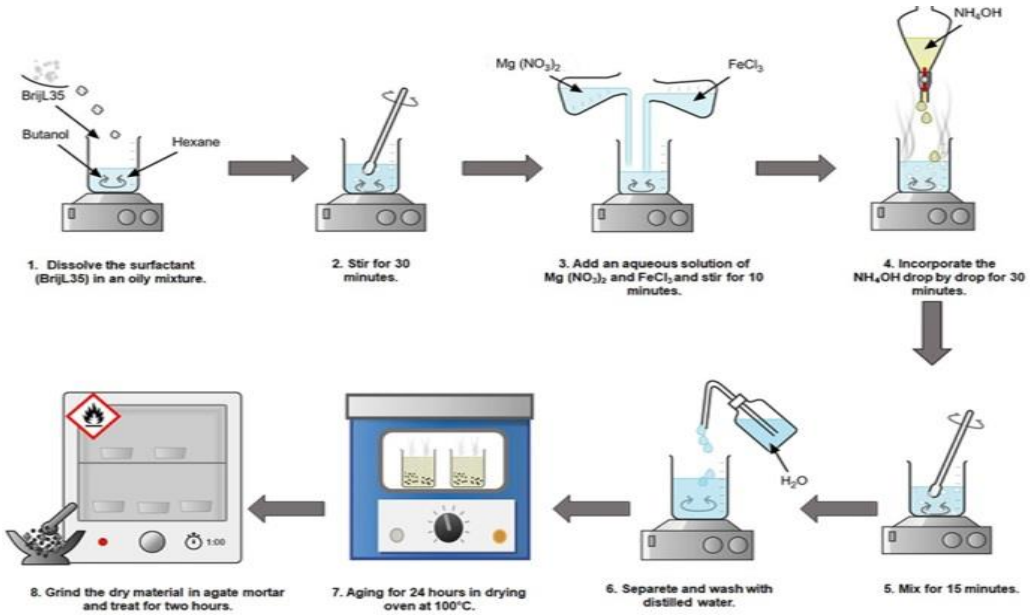

Figure 1. Microemulsion method: synthesis of magnesium nanoferrites ($MgFe_2O_4$).

2.3 Characterization of $MgFe_2O_4$ nanoparticles

The morphological characteristics and elemental composition of the chemical species were analyzed with a JSM-6610LV scanning electron microscope (SEM-EDX) using backscattered electrons and a voltage of 30 kV. Transmission electron microscopy was employed to examine the morphology, particle size, and diffraction patterns (TEM, Titan 80-300 kV). The magnetic properties (Ms, Mr, and Hc) were characterized using vibrating sample magnetometry (VSM, Quantum Design, 6000) at room temperature with a constant magnetic field intensity of 20 KOe.

The heat-treated particles were analyzed via X-ray diffraction (XRD) using a Philips 3040 X-ray diffractometer with Cukα radiation (1.54 Å), operating at a scanning rate of 0.2°/s.

Thermal analysis was conducted using a Model Q 500 thermogravimetric and differential thermal analyzer (TGA-DSC), with approximately 20 mg of each sample. The samples were heated from room temperature to 1000 °C under controlled conditions, with a heating rate of 15 °C/min.

Cell viability was determined visually using a Neubauer chamber. A cell suspension was made with whole blood and physiological solution at a dilution of 4X, subsequently the sample was added to the counting area (10 µL), then the sample was left to rest in the chamber for a minute before finally being placed under the microscope. Suspension of the cells was prepared using a concentration (cell/ml) = (number of cells / 4) (dilution factor).

2.4 Magnetic induction of $MgFe_2O_4$ nanoparticles

A solid-state magnetic induction device (Ambrell Easy Heat 0224) was employed to assess the heating capacity of the magnetic nanoparticles. Aqueous suspensions containing 6, 8, 10, and 12 mg of nanoparticles in 1 ml of deionized water were prepared and subjected to a magnetic field of 10.2 kA/m and a frequency of 354 kHz for 10 minutes. The specific absorption rate (SAR) was determined using the following equation:

$$SAR = \frac{C}{w} * \frac{\Delta T}{\Delta t} \quad \textbf{(Eq. 1)}$$

Where w is the weight of the magnetic material, ΔT/Δt is the total slope of the temperature vs. time curve, and C is the specific heat of the medium in which particles are suspended (H_2O = 4.1868 J/g).

3. Results and discussion

3.1 XRD studies of $MgFe_2O_4$ nanoparticles

Figure 2 shows the XRD patterns of the obtained nanoparticles. The diffraction peaks observed correspond to the (220), (311), and (400) planes, according to JCPDS 36-0398 for magnesium ferrite ($MgFe_2O_4$), indicating the formation of a face-centered cubic $MgFe_2O_4$ structure. The XRD patterns of the samples exhibited distinct primary peaks characteristic of magnesium ferrite nanoparticles at 2θ = 30.29, 35.45, 43.35, 53.53, 57.25, and 62.66, which correspond to the (220), (311), (400), (422), (511), and (440) crystal planes of $MgFe_2O_4$, respectively. These results are in agreement with those reported by Bouzidi *et al.* [16]. The formation of the pure magnesium ferrite phase is promoted when the magnesium content reaches a ratio of Mg x = 1. In contrast, lower magnesium levels lead to the presence of diffraction peaks associated with iron oxide, corresponding to the hematite phase. The reaction medium employed, along with higher iron concentrations, facilitated the formation of the hematite phase during synthesis.

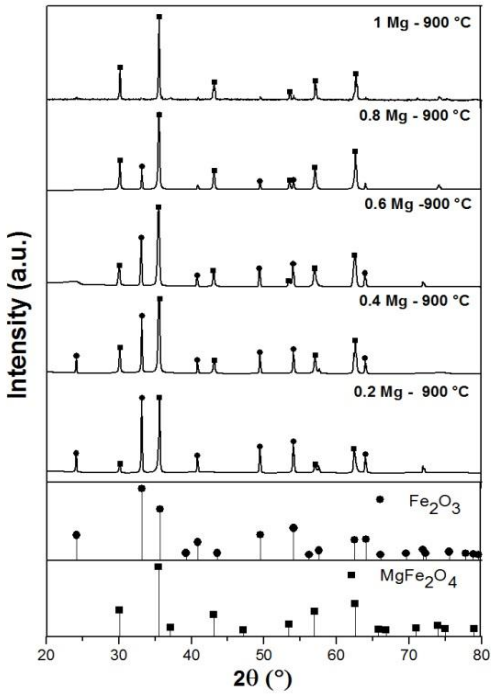

Figure 2. Diffraction patterns of $Mg_xFe_{3-x}O_4$ nanoparticles treated at 900 °C.

Table 1. Percentage of phases present in $Mg_xFe_{3-x}O_4$ nanoparticles.

Sample	Fe_2O_3	$MgFe_2O_4$
$Mg_{0.2}Fe_{2.8}O_4$	13%	87%
$Mg_{0.4}Fe_{2.6}O_4$	14%	86%
$Mg_{0.6}Fe_{2.4}O_4$	9%	91%
$Mg_{0.8}Fe_{2.2}O_4$	3%	97%
$Mg_1Fe_2O_4$	0	100%

3.2 TGA-DSC studies of $MgFe_2O_4$ nanoparticles

The thermal analysis of the precursors is shown in Figure 3. A slight weight reduction is observed from room temperature up to approximately 100°C, attributed to the evaporation of solvent and water absorbed during synthesis. As the temperature exceeds 150°C, further weight losses occur, beginning around 190°C and 230°C, and continuing until near 500°C. These losses are associated with residual products from the reaction, such as carbon chains, dodecane, and ammonium, which decompose at approximately 230°C and 240°C, respectively. The total weight loss

is around 50%. DSC analysis revealed the release of energy from the sample. Distinct peaks, both exothermic and endothermic, indicate the evaporation and chemical decomposition of the organic precursors used during the synthesis process. The crystallographic transition is responsible for an exothermic peak observed at around 450 °C. According to a study conducted by Orhan *et al.* [17], the microemulsion procedures generate waste products, such as ammonium and carbon chains, which are eliminated through washing and heat treatments. These compounds are responsible for the exothermic peaks observed [16][18].

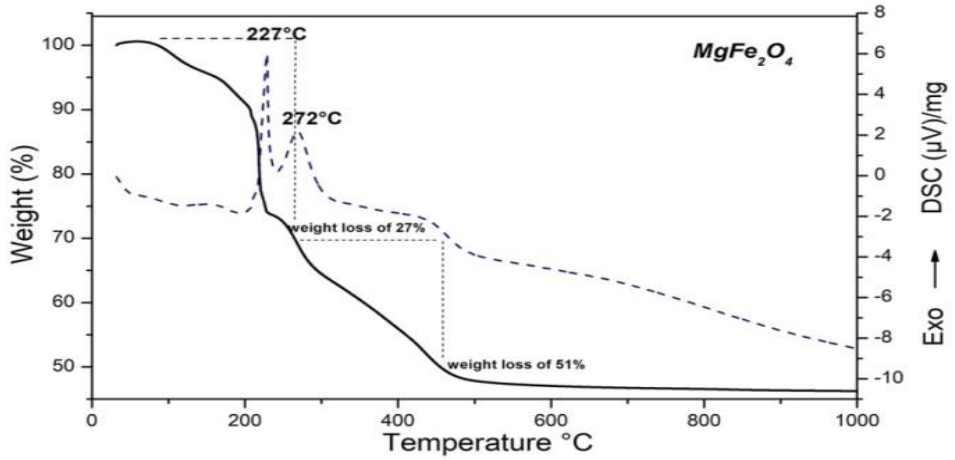

Figure 3. Thermogram (TGA-DSC) of the precursor of $MgFe_2O_4$ nanoparticles.

3.3 SEM-EDX studies of $MgFe_2O_4$ nanoparticles

Figure 4 shows the SEM micrograph and EDX spectrum for the sample heat-treated at 900 °C, which corresponds to the sample containing the pure magnesium ferrite phase (Fe: Mg, 2:1). The micrograph obtained by SEM shows aggregates with varied morphology and sizes between 5 and 20 µm, M. Junaid *et al*. [19] report similar behavior as a consequence of nanoparticle agglomeration. The agglomeration is believed to occur due to the high surface energy of nanoscale particles. EDX analysis reveals the presence of only Mg, Fe, and O, with no traces of elements from the reaction [20].

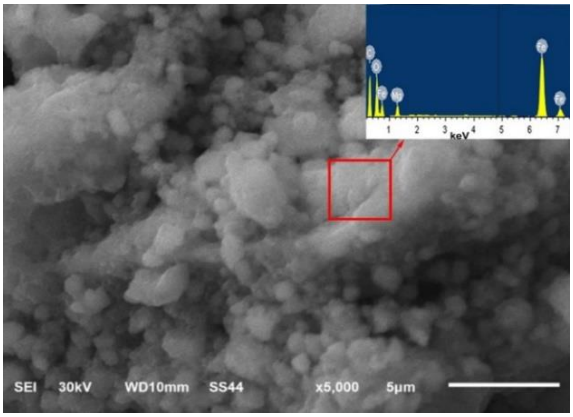

Figure 4. $MgFe_2O_4$ nanoparticles: SEM image and EDX spectrum.

3.4 TEM-HRTEM-SAED studies of $MgFe_2O_4$ nanoparticles

The TEM images depicted in Figure 5 show $MgFe_2O_4$ nanoparticles synthesized by microemulsion and thermally treated at 900 °C. This sample was selected because it represents a pure phase. The particles exhibit an irregular morphology, appearing closed together and compact. Due to the magnetic

attraction between the nanoparticles, they tend to form agglomerates, as seen in Figure 5a. The nanoparticles' large specific surface area, high chemical reactivity, and inherent dipolar magnetic interactions, as they are characterized as monodomain, make them prone to oxidation and agglomeration. The analysis of selected area electron diffraction (SAED) confirms the formation of $FeMg_2O_4$, image 5b, while the analysis of high-resolution transmission electron microscopy (HRTEM-SAED) observed in image 5c corroborates that the reflections presented correspond to the crystallographic patterns (220) and (311), which were obtained from their experimental interplanar distances d = 2.969 and 2.521, respectively, corresponding to the magnesium ferrite, according to the crystallographic chart (JCPDS: 04-008-2382). Finally, the histogram in Figure 5d shows a particle size distribution from 100 individual counts, obtaining an average size of 31 nm. Therefore, it can be confirmed that the materials produced using this synthesis method are within the nanoscale range [21] [22].

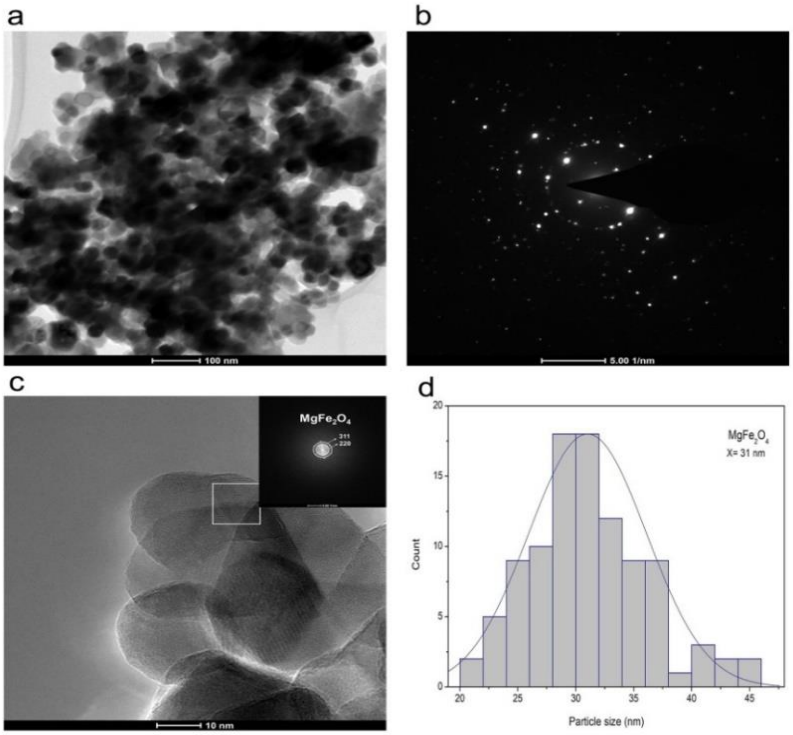

Figure 5. $MgFe_2O_4$ nanoparticles images: a) TEM, b) SAED, c) HRTEM-SAED, d) particle size distribution histogram.

3.5 VSM studies of $MgFe_2O_4$ nanoparticles

Figure 6 illustrates the hysteresis loops and magnetic properties of nanoparticles with varying stoichiometric ratios of magnesium, with the pure phase observed at 900 °C. The hysteresis loops exhibit the typical curve for superparamagnetic behavior (no open loops), with coercivity near zero [23].

A monodomain system forms when the size of a ferritic or ferromagnetic material is smaller than a domain, which is the region where the material's spins are aligned in a single direction. These domains have a defined (micrometric) size. When a new magnetic behavior emerges, it is referred to as super-para-magnetism. Superparamagnetic behavior occurs when the particle size is below 100 nm. Given that the average particle

size measured by TEM was 31 nm for magnesium ferrite, this demonstrates the material's superparamagnetic behavior [23] [24].

The values of magnetic properties were estimated at 18.419 emu/g and 8.790 emu/g for saturation magnetization (Ms). While 0.468–1.712 emu/g for remnant magnetization (Mr) and 0.005–0.019 Oe for coercivity (Hc), the Ms values show a slight variation and are attributed to different stoichiometric ratios of magnesium in the $MgFe_2O_4$ nanoparticles. These values increased as the amount of magnesium increased, ranging from 8.79 to 18.42 emu/g.

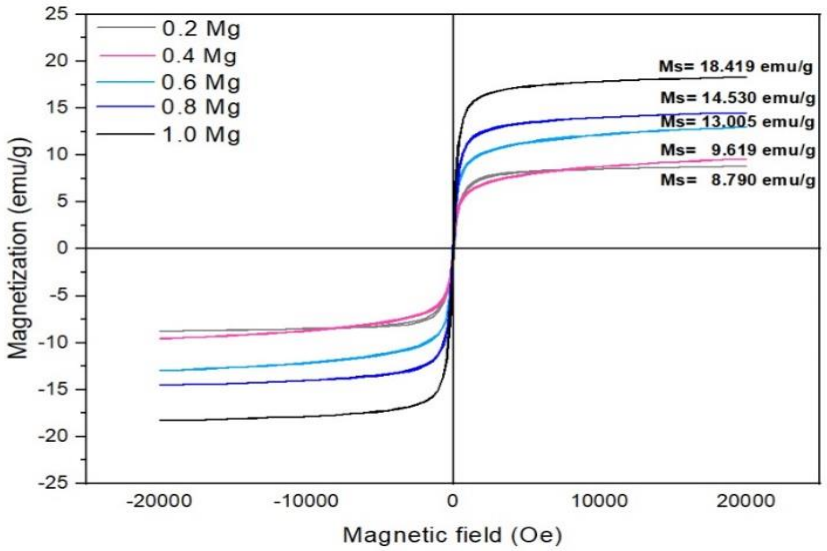

Figure 6. $Mg_xFe_{3-x}O_4$ nanoparticles' hysteresis loops and magnetic values.

Table 2 presents the magnetic properties of the MgFe204. The highest saturation magnetization (Ms) values are found in the sample with 2:1 Fe: Mg. The differences in magnetic parameters can be attributed, according to some authors, to exchange interactions between ions in the network [25]. These variations are also influenced by particle size and the anisotropy constant. The synthesized nanoparticles are smaller than 100 nanometers in size. Studies, such as those conducted by J. Uddin and Y. Jeong [26], have confirmed the impact of Mg and Fe ratios on the properties of magnesium ferrites. Non-magnetic cations such as Mg^{+2} occupy tetrahedral voids, as in ordinary spinels, forcing the movement of Fe^{+3} out of tetrahedral voids into octahedral sites, where they align, thus increasing the magnetization of the material. The presence of the iron oxide phase leads to a reduction in magnetization values in samples with lower magnesium content (Fe_2O_3) [21] [18].

Table 2. Magnetic properties of $Mg_xFe_{3-x}O_4$ nanoparticles.

Sample	Ms (emu/g)	Mr (emu/g)	Hc (Oe)
$Mg_{0.2}Fe_{2.8}O_4$	8.790	0.468	0.005
$Mg_{0.4}Fe_{2.6}O_4$	9.619	0.720	0.004
$Mg_{0.6}Fe_{2.4}O_4$	13.005	1.001	0.005
$Mg_{0.8}Fe_{2.2}O_4$	14.530	1.657	0.009
$Mg_1Fe_2O_4$	18.419	1.712	0.019

3.6 Magnetic induction of $MgFe_2O_4$ nanoparticles

The heating capacity results are shown in Figure 7. $Mg_xFe_{3-x}O_4$ nanoparticles with Fe: Mg ratios of 2:1, 2.2:0.8, 2.4:0.6, 2.6:0.4and 2.8:0.2 were heat treated at 900 °C. These results indicate that the suspension containing magnesium ferrite with a stoichiometric ratio of 2:1 (Fe: Mg) exhibited the highest heating capacity, reaching a temperature of 43.5°C in 152 seconds. This temperature is considered optimal for promoting the destruction of cancerous tissue in hyperthermia therapy. Ferrites with a stoichiometric ratio other than 2:1 show no heating capacity above 40°C in 600 seconds, a phenomenon that can be inferred from the presence of Fe_2O_3 as an additional antiferromagnetic phase and responsible for the decrease in saturation magnetization values, according to the results obtained by XRD and VSM.

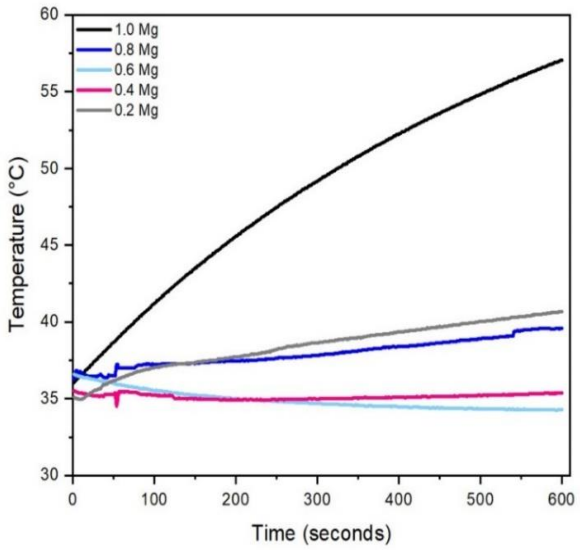

Figure 7. Heating capacity of $Mg_xFe_{3-x}O_4$ nanoparticles under the application of the magnetic field.

Different nanoparticle solutions were investigated, considering the values found for the heating capacity of $Mg_xFe_{3-x}O_4$ nanoparticles with Fe: Mg ratios of 2:1. The results are presented in Figure 8. The suspensions were dispersed in water at concentrations of 6, 8, 10, and 12 mg/ml to evaluate their heating capacity. The results show that the nanoparticles were capable of increasing the suspension temperature from 44°C to 64°C within 600 seconds. These temperatures fall within the suitable range for hyperthermia therapy, which aids in the destruction of cancer tissue, as such cells are sensitive to temperature variations and undergo apoptosis when exposed to temperatures above 41–45° [27] [26].

The hyperthermia process induced by nanoparticles is associated with two phenomena: Brownian and Néel relaxations. These relaxation processes disrupt the alignment of magnetic moments when nanoparticles are immersed in a liquid, either due to the physical rotation of particles in the solution (Brownian relaxation) or the thermal randomness of the magnetic moments (Néel relaxation). While Néel relaxations and the hysteresis process are independent of the surrounding environment, Brownian relaxation is influenced by the viscosity of the medium, which may change under biological conditions. Superparamagnetic particles can exist as single-domain particles, and hysteresis losses may become significant at sufficiently high field amplitudes [28].

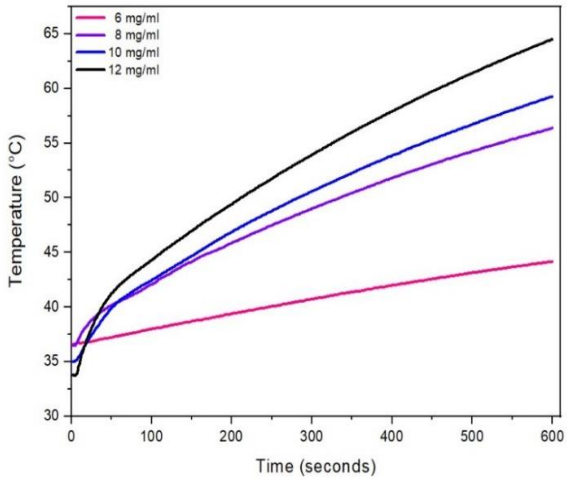

Figure 8. Heating capacity of different suspensions of $MgFe_2O_4$ nanoparticles under the application of the magnetic field.

To heat tissues, the specific absorption rate (SAR) is linked to the amount of heat absorbed. This concept refers to the amount of thermal energy lost per unit mass of magnetic material in the sample when exposed to an alternating current (AC) magnetic field. Table 3 presents the SAR values and maximum temperatures. The nanoparticle suspensions prepared contained 6, 8, 10, and 12 mg in 1 ml of water.

The maximum temperatures reached and the calculated SAR values suggest that all the suspensions have potential for use in hyperthermia treatment. The SAR values and heating temperatures of the 6 mg/ml suspension are classified in the literature as moderate hyperthermia, which is used to enhance tumor sensitivity to radiation and chemotherapy [22]. The thermal ablation is used to directly induce cell death by necrosis (50 °C), as is the case with the suspension of 8,10, and 12 mg/ml [28]. The sample of 6 mg/ml is a suitable choice to show a lower level of damage to the organism.

SAR values result from dipolar interactions that are influenced by the size of nanoparticle clusters, with iron oxides showing therapeutic SAR values between 25 and 75 W/g. Tong *et al.* [22] also refer to values between 10 kA/m and 100 kHz, respectively. Cardoso *et al.* [29] synthesized nanoparticles of calcium-substituted magnesium ferrite by the co-precipitation method, obtaining SAR values between 12 and 46 W/g. The SAR values found in this research (5.7-26.4 W/g) are within the above-mentioned ranges. Based on the results, magnesium ferrite nanoparticles are ideal candidates for hyperthermia therapy, as they reach a temperature of 43.5°C after approximately 150 seconds. Hyperthermia is employed to enhance tumor sensitivity to radiation and chemotherapy, while thermal ablation, which involves temperatures above 50°C, leads to direct cell death through necrosis. Thus, these samples can be used for both purposes, with the exposure time to the magnetic field adjusted as needed [30] [31].

Table 3. SAR values, maximum temperature reached and $\Delta T/\Delta t$ of nanoparticles suspensions $MgFe_2O_4$.

Mass (mg)	Maximum temperature reached (°C)	ΔT/Δt (°C/s)	SAR total (W/g)
6	44.32	0.0630	5.7587
8	56.08	0.0516	16.2041
10	59.13	0.0386	21.6343
12	64.21	0.0137	26.4067

3.7 Cell viability

To demonstrate cell viability, suspensions of erythrocyte cells (at concentrations of 10 mg/ml) were used sample with a Fe: Mg = 2:1 stoichiometric ratio calcinated a 900 °C. The apoptosis rate in all concentrations was different from the control group in barely perceptible percentages; the control was used as a means of comparison by having all samples in the same fluid but without the presence of nanoparticles. Figure 9 shows the percentages obtained for the cell viability. During the first 24 hours, the percentage was higher than 94%. After 36 hours, the percentage of living cells was 85%. Then, 48 hours later, cell viability was reduced to approximately 77%. Finally, at 60 hours, cell viability was less than 60%, something natural that occurs in all cells after that time when they are extracted from the body due to a lack of nutrients. Previous studies have shown the cytotoxicity of various dose-dependent ferrites [32] [33] where the number of deaths varies according to the pathophysiology, exposure period, cell type, and exposure concentration. It is debatable to

claim and contrast cytotoxicity studies carried out on healthy cells and cancer cells because cancer cells are more vulnerable to death from external factors.

About magnesium ferrites, it can be stated that, specifically those obtained in the present research, are not cytotoxic due to their biocompatible components. Iron, magnesium, and oxygen are a few of the bioelements found in the body. It is possible to observe in the graph that the dotted line shows 50% cell viability, which determines that all the suspensions analyzed were viable for the erythrocyte even after 60 hours of exposure, indicating the cellular stability of erythrocytes in the presence of magnesium ferrite nanoparticles [8] [34].

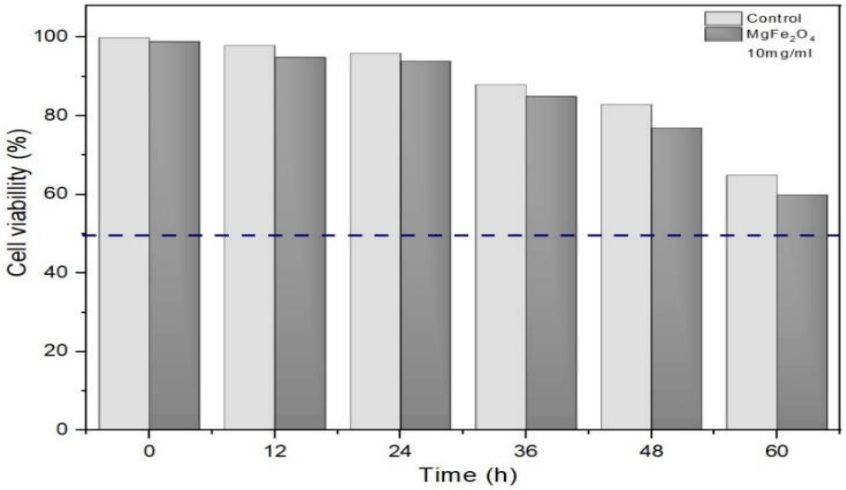

Figure 9. Cell viability of $MgFe_2O_4$ with erythrocyte cells.

4. Conclusions

Nanoparticles can be utilized in anticancer therapies like magnetic hyperthermia, but they must possess specific characteristics, including a particle size in the nanometer range, superparamagnetic behavior, and the ability to generate heat when exposed to a magnetic field via induction. To effectively destroy cancer cells in the body, the temperature must range between 40 and 43 degrees Celsius. This study emphasizes the potential of magnesium ferrite nanoparticles, synthesized through a wet method, in antitumor therapies such as magnetic hyperthermia treatments.

The formation of the crystalline phase of magnesium ferrite began at approximately 450°C. At a stoichiometric ratio of 2:1 (Fe: Mg) and 900°C, X-ray diffraction analysis showed the presence of magnesium ferrite without any secondary phases. The thermograms obtained for the precursors of $MgFe_2O_4$ showed an average loss of 51% of the weight of the samples. Apply a heat treatment at 450 °C to the crystalline phase of the magnesium ferrite. "SEM micrographs of uncoated ferrites revealed some agglomeration, with agglomerate sizes ranging from 5 to 20 μm. TEM analysis showed the presence of nanoparticles with an average size of 31 nm. This particle size directly influenced the magnetic properties, resulting in superparamagnetic behavior with a maximum saturation magnetization of 18.32 emu/g, and coercivity and remanence near zero. Heat capacities above 43.5°C and specific absorption rates between 5.7 and 26.4 W/g were achieved at a frequency of 10.2 kA/m and 350 kHz. Cytotoxicity levels for erythrocyte cells in the presence of magnesium ferrites were up to 60 hours

higher than 50% and very close to the control used. Thus, the nanoparticles produced in this study have potential applications in magnetic hyperthermia treatment.

5. Acknowledgments

This research has been supported by the Tecnológico Nacional de México through the research academic group ITSAL-CA-12 and the research project 21880.25P. Author Carolina García Feria with CVU 1000701 is indebted to SECIHTI for financial support in the form of a scholarship for doctorate studies.

References

[1] A. R. K. Santhiya R, "Role of metal oxide ferrites in the process of magnetic hyperthermia", *J. Therm. Biol.*, 2024.

[2] P. S. Mkwae *et al.*, "Insightful acetone gas sensing behaviour of Ce substituted MgFe2O4 spinel nano-ferrites", *J. Mater. Res. Technol.*, vol. 9, no. 6, pp. 16252–16269, 2020, doi: 10.1016/j.jmrt.2020.11.079.

[3] A. M. Jumaa, M.B., Mubarak, T.H. & Mohammad, "Exploring Cu-substituted Zn nanoferrites: synthesis, structural, magnetic, morphological, and antibacterial properties", *J Sol-Gel Sci Technol*, 2022, [Online]. Available: https://doi.org/10.1007/s10971-025-06742-4.

[4] G. M. M. Frausto Gascón, Juan Salvador, Alexa Yael García-Fimbres, Celia Paola Gutierrez Aranda, Ximena Dannae Hernández Muñoz, Paola OrozcoF ernández, Teresa Alejandra Razo Lazcano, "Síntesis De nanopartículas De Oro Utilizando Nano-Emulsiones Y Extractos Naturales Como Agentes Reductores", *Jovenes en la Cienc. 21*, 2023, [Online]. Available: https://www.jovenesenlaciencia.ugto.mx/index.php/jovenesenlaciencia/article/view/3943.

[5] D. A. B. Chetan Pandit, Arpita Roy, Suresh Ghotekar, Ameer Khusro, Mohammad Nazmul Islam, Talha Bin Emran, Siok Ee Lam, Mayeen Uddin Khandaker, "Biological agents for synthesis of nanoparticles and their applications", *J. King Saud Univ. - Sci.*, vol. 101869, no. ISSN 1018-3647, 2022, doi: https://doi.org/10.1016/j.jksus.2022.101869.

[6] D. et al. Malik, A.Q., Mir, T.u.G., Kumar, "A review on the green synthesis of nanoparticles, their biological applications, and photocatalytic efficiency against environmental toxins", *Env. Sci Pollut Res 30*, vol. 69796–6982, 2023, doi: https://doi.org/10.1007/s11356-023-27437-9.

[7] H. H. and Z. G. Zhang D, Ma X-l, Gu Y, "Green Synthesis of Metallic Nanoparticles and Their Potential Applications to Treat Cancer", *Front. Chem*, vol. 8, 2020, doi: https://doi.org/10.3389/fchem.2020.00799.

[8] C. Guyton and J. Hall, *Guyton Y Hall Tratado De Fisiología Médica John E. Hall*, vol. 14a. 2021.

[9] T. Pulingam, P. Foroozandeh, J. Chuah, and K. Sudesh, "Exploring Various Techniques for the Chemical and Biological Synthesis of Polymeric Nanoparticles", 2022, doi: DOI:10.3390/nano12030576.

[10] Ana Ketzaly Calvillo Anguiano,

"Evaluación de la viabilidad celular y la actividad antimicrobiana de nanopartículas de cobre Tesis". 2019, [Online]. Available: http://www.fc.uaslp.mx/pca/tesis/2019Maestria/CalvilloAnguianoAnaKetzaly-Maestria201989.pdf.

[11] Z. V. Cancino J, Marangoni V.S, "Nanomedicine, Nanoscience and its applications", *Elsevier*, pp. 71–84, 2017, doi: https://doi.org/10.1016/B978-0-323-49780-0.00003-X.

[12] F. A. S. da Silva and M. F. de Campos, "Study of heating curves generated by magnetite nanoparticles aiming application in magnetic hyperthermia", *Brazilian J. Chem. Eng.*, vol. 37, no. 3, pp. 543–553, 2020, doi: 10.1007/s43153-020-00063-5.

[13] J. K. Man Shu, Jingguang Wang, Ziyang Xu, Teliang Lu, Yue He, Renshan Li, Guoqing Zhong, Yunbo Yan, Yu Zhang, Xiao Chu, "Targeting nanoplatform synergistic glutathione depletion-enhanced chemodynamic, microwave dynamic, and selective-microwave thermal to treat lung cancer bone metastasis", *ioactive Mater.*, vol. 39, pp. 544–561, 2024, doi: https://doi.org/10.1016/j.bioactmat.2024.04.016.

[14] Y. Lu, W. Dong, J. Ding, W. Wang, and A. Wang, "Hydroxyapatite Nanomaterials: Synthesis, Properties, and Functional Applications", *Nanomater. from Clay Miner.*, pp. 485–536, 2019, doi: 10.1016/B978-0-12-814533-3.00010-7.

[15] A. Ravi, Rangnath, Mishra and S. Anamika, Ahmad, "Fabrication of Superparamagnetic Bimetallic Magnesium Nanoferrite Using Green Polyol: Characterization and Anticancer Analysis in Vitro on Lung Cancer Cell Line A549", *Am. Chem. Soc.*, vol. 5, 2022, doi: doi: 10.1021/acsabm.2c0072910.1021/acsabm.2c00729.

[16] M. G. & J. J. Souhir Bouzidi, Najah Rhimi, Jamila Dhahri, Zouhaier Aloui, Abdelaziz Bouazizi, Kamel Khirouni, "Eu-doped Mg–Ni ferrites: a reliable strategy to enhance dielectric properties for high-frequency applications", *J Mater Sci Mater Electron*, vol. 36, p. 32, 2025, doi: https://doi.org/10.1007/s10854-024-14058-2.

[17] G. Orhan, Z., Daş, E. & Bozkurt, "Microemulsion synthesis of SnO2 nanoparticles and their integration in Au/n-Si/Al device structure", *J Mater Sci Mater Electron*, vol. 36, p. 158, 2025, doi: https://doi.org/10.1007/s10854-025-14242-y.

[18] M. Tadic, J. Lazovic, M. Panjan, and S. Kralj, "Hierarchical iron oxide nanocomposite: Bundle-like morphology, magnetic properties and potential biomedical application", *Ceram. Int.*, vol. 48, no. 11, pp. 16015–16022, 2022, doi: 10.1016/j.ceramint.2022.02.145.

[19] M. Junaid *et al.*, "Structural , spectral , dielectric and magnetic properties of indium substituted copper spinel ferrites synthesized via sol gel technique", *Ceram. Int.*, no. June, pp. 1–9, 2020, doi: 10.1016/j.ceramint.2020.07.227.

[20] A. B. K. Arun V. Bagade, Sangita N. Pund, Pratik A. Nagwade, Brajesh Kumar, Satish U. Deshmukh, "Ni-

doped Mg-Zn nano-ferrites: Fabrication, characterization, and visible-light-driven photocatalytic degradation of model textile dyes", *Catal. Commun.*, vol. 181, 2023, doi: https://doi.org/10.1016/j.catcom.2023.106719.

[21] M. D. S. Moya Carlos Ferrer Giménez, Vicente Amigó Borrás, "Fundamentos de ciencia de los materiales", *Universidad politecnica de Valencia*. 2023, [Online]. Available: https://www.upv.es/materiales/Fcm/Indice_FCM.html.

[22] S. Tong, H. Zhu, and G. Bao, "Magnetic iron oxide nanoparticles for disease detection and therapy", *Mater. Today*, vol. 31, no. xx, pp. 86–99, 2019, doi: 10.1016/j.mattod.2019.06.003.

[23] M. Tadic, S. Kralj, and L. Kopanja, "Synthesis, particle shape characterization, magnetic properties and surface modification of superparamagnetic iron oxide nanochains", *Mater. Charact.*, vol. 148, no. December 2018, pp. 123–133, 2019, doi: 10.1016/j.matchar.2018.12.014.

[24] L. Kopanja, M. Tadić, S. Kralj, and J. Žunić, *Shape and aspect ratio analysis of anisotropic magnetic nanochains based on TEM micrographs*, vol. 44, no. 11. Elsevier Ltd and Techna Group S.r.l., 2018.

[25] T. Tatarchuk *et al.*, "Magnesium-zinc ferrites as magnetic adsorbents for Cr(VI) and Ni(II) ions removal: Cation distribution and antistructure modeling", *Chemosphere*, vol. 270, 2021, doi: 10.1016/j.chemosphere.2020.129414.

[26] J. Uddin and Y. Jeong, "Chemosphere Application of magnesium ferrite nanomaterials for adsorptive removal of arsenic from water : Effects of Mg and Fe ratio", *Chemosphere*, vol. 307, no. P3, p. 135817, 2022, doi: 10.1016/j.chemosphere.2022.135817.

[27] H. Z. Feng Ding, Guobin Qiu, Fengliang Tan, Tengyan Wu, Longzhen Ding, Xin Liu, "Preparation and characterization of PEGylated magnetic ferrite with a biocompatible delivery for DOX", *Appl. Phys. A*, vol. 12, p. 129, 2023, doi: https://doi.org/10.1007/s00339-023-07160-5.

[28] V. Vilas-Boas, F. Carvalho, and B. Espiña, "Magnetic hyperthermia for cancer treatment: Main parameters affecting the outcome of in vitro and in vivo studies", *Molecules*, vol. 25, no. 12, pp. 1–30, 2020, doi: 10.3390/molecules25122874.

[29] B. D. Cardoso *et al.*, "Magnetoliposomes based on shape anisotropic calcium/magnesium ferrite nanoparticles as nanocarriers for doxorubicin", *Pharmaceutics*, vol. 13, no. 8, 2021, doi: 10.3390/pharmaceutics13081248.

[30] G. Nandhini and M. K. Shobana, "Efecto de la moringa oleifera con nanoferritas de Mn y Ni puras y dopadas con Zn para aplicaciones de hipertermia," *Mater. Today Commun.*, vol. 39, 2024, doi: https://doi.org/10.1016/j.mtcomm.2024.109046.

[31] Marta Vassallo, Daniele Martella, Gabriele Barrera, Federica Celegato, Marco Coïsson, Ricardo Ferrero, Elena S. Olivetti, Adriano Tróia, Hüseyin Sözeri, Camilla Parmeggiani,

Diederik S. Wiersma, Paola Tiberto and A. Manzin, “Mejora de las propiedades de hipertermia de las nanopartículas de óxido de hierro mediante recubrimiento superficial”, *ACS Omega*, vol. 8, 2023, [Online]. Available: https://pubs-acs-org.translate.goog/doi/10.1021/acsomega.2c06244?_x_tr_sl=en&_x_tr_tl=es&_x_tr_hl=es&_x_tr_pto=tc.

[32] S. Kanagesan *et al.*, “Evaluation of antioxidant and cytotoxicity activities of copper ferrite (CuFe2O4) and zinc ferrite (ZnFe2O4) nanoparticles synthesized by sol-gel self-combustion method”, *Appl. Sci.*, vol. 6, no. 9, pp. 1–13, 2016, doi: 10.3390/app6090184.

[33] A. Rafieepour *et al.*, “Investigation of the effect of magnetite iron oxide particles size on cytotoxicity in A549 cell line”, *Toxicol. Ind. Health*, vol. 35, no. 11–12, pp. 703–713, 2019, doi: 10.1177/0748233719888077.

[34] K. Shahzad *et al.*, “Effect of Magnesium Substitution on Structural, Magnetic and Biological Activity of Co(1-x)Mg(x)Fe2O4 Nano-colloids”, *J. Clust. Sci.*, vol. 32, no. 4, pp. 1003–1014, 2021, doi: 10.1007/s10876-020-01862-z.